PHYSICAL REVIEW D VOLUME 40, NUMBER 4 15 AUGUST 1989

Dynamics of thick domain walls

Lawrence M. Widrow
Department of Physics, Harvard University, Cambridge, Massachusetts 02138
and Harvard-Smithsonian Center for Astrophysics, 60 Garden Street, Cambridge, Massachusetts 02138
(Received 13 April 1989)

The dynamics of thick domain walls are studied in the context of the classical field theory for a real scalar field. We treat, by numerically solving the equation of motion for the scalar field, the collision of two plane-symmetric walls as well as the collapse of walls that have spherical and cylindrical symmetry. Walls in both sine-Gordon and ϕ^4 theories are considered. We illustrate the striking and at times surprising differences between thin and thick walls. We also discuss the formation of black holes during spherical collapse.

I. INTRODUCTION

Recently, Hill, Schramm, and Fry[1] (HSF) suggested that very light or "soft" domain walls might be the seed energy-density fluctuations necessary to initiate the formation of large-scale structure. In addition, Stebbins and Turner[2] proposed that a single domain wall stretching across our Hubble volume might be responsible for the large-scale bulk motion observed in our local neighborhood.[3] In the HSF scenario, domain walls form during a late-time phase transition that occurs after matter and radiation have decoupled. The walls lead to large energy-density fluctuations ($\delta\rho/\rho \sim 1$) that immediately grow nonlinearly. Structures could, therefore, form by redshift $z \geq 3$ as is required to explain the existence of quasars observed at these redshifts. Furthermore, HSF argue that the distortions in the microwave background induced by the walls are small and can be well within observational limits.

This renewed interest in domain walls prompted us to consider their dynamics in some detail. Most of the previous work on domain walls has made use of the thin-wall approximation. A wall of negligible thickness is most easily treated as a $(2+1)$-dimensional hypersurface. The equations of motion for the wall are determined by minimizing the area of this hypersurface (see, for example, Ref. 4) much as the Nambu-Goto equations of motion for a string are determined by minimizing the area of the $(1+1)$-dimensional world surface swept out by the string. In the thin-wall approximation, a number of problems can be treated analytically.[5-7]

Presently, we study the dynamics of "realistic" (i.e., thick) domain walls. Though motivated by the recent work of HSF, our analysis is completely general and therefore applicable to domain walls occurring at any stage in the history of the Universe. As we shall see, there are some rather surprising differences between thick and thin walls.

Cosmic domain walls form when a discrete symmetry is spontaneously broken. Simply put, walls form the boundaries between regions of the Universe that have settled into distinct vacuum states. In the simplest models, symmetry breaking is accomplished by a real scalar field Φ, where Φ acquires different vacuum expectation values (VEV's) in different regions of the Universe. Walls occur where Φ changes from one VEV to another; that is, where Φ is in a false-vacuum state. The thickness of the wall is determined by balancing gradient and potential energies, i.e., by solving the equations of motion for Φ. Likewise, the dynamics of the wall are determined by solving these equations. In this respect, the wall is nothing more than a special configuration of the Φ field. (A similar approach is taken by Press, Ryden, and Spergel[8] in their simulations of cosmic domain-wall networks.)

Before discussing the present work, let us review what is known about cosmological domain walls. At the time of formation, there are both infinite and closed surface walls.[8-10] The evolution of the system once the domain walls have formed is complicated and very model dependent and a complete understanding of cosmological domain walls is out of reach. It is, nevertheless, useful to list the forces that come into play. The stress energy of a wall is composed of a surface energy density and surface tension equal in magnitude to the surface energy. Because of the tension, closed walls collapse and regions in infinite walls with small-scale irregularities oscillate. On the other hand, large-scale features (i.e., features with curvature scales greater than the Hubble length) are conformally stretched by the cosmological expansion. In addition, there are processes which damp the motion of the walls. For example, particles that are reflected by the wall exert a frictional force which damps motion of the walls relative to the cosmic rest frame. More important perhaps are the energy-loss mechanisms such as gravitational and particle radiation which damp out small-scale irregularities in infinite walls and cause closed surface walls to eventually disappear. As a final note, we mention the possibility that a closed surface wall can collapse to form a black hole.

In the present work, we consider the dynamics of some very simple wall configurations focusing on the scalar field Φ and neglecting the coupling of Φ to gravity and to other fields. Our analysis is, therefore, sensitive only to the effects of surface tension and Φ-particle radiation. As

 ©1989 The American Physical Society

discussed above, we do not solve for the motion of the walls *per se* but rather for the evolution of the Φ field. This is done using a one-dimensional partial differential equation code and we are, therefore, limited to spherical, cylindrical, and plane-symmetric walls. The advantage of a one-dimensional code is, of course, that we can use an extremely fine grid and therefore obtain very accurate simulations. Furthermore, the three problems accessible to our code roughly correspond to spherical, cigar-shaped, and pancake-shaped walls, the three shapes one generally expects for closed surface walls in a domain-wall network.

Though our analysis is somewhat limited, the results, we believe, will be important in understanding the evolution of a system of domain walls and the role walls may play in structure formation. For example, we discuss in some detail, the loss of energy due to Φ-particle radiation during spherical and cylindrical collapse. If closed walls are to act as seeds for structure formation then it is essential that they live for a long time, i.e., that the energy loss due to particle radiation be small. As we shall see, the fraction of energy lost to radiation depends on the details of the Φ-fields potential and on T/R_0, where T is the thickness of the wall and R_0 is the maximum radius of the wall (i.e., $R=R_0$ for $dR/dt=0$). A second issue of cosmological importance addressed is the collapse of a spherical wall into a black hole. Though gravity has been neglected, it is still possible to make some qualitative predictions about black-hole formation. Our results indicate that black holes can form even for the soft walls considered by HSF.

An outline of the paper is as follows. In Sec. II we briefly review the properties of domain walls relevant to the present work. (For a more complete review of the basic properties of domain walls, see Ref. 4.) In Sec. III we discuss the numerical simulations, paying particular attention to a host of tests conducted to verify the validity of the code. In Sec. IV we discuss the results in more detail and in Sec. V we give a summary of our work and discuss implications for cosmological domain-wall scenarios.

II. GENERAL PROPERTIES OF DOMAIN WALLS

Consider the theory of a real scalar field $\Phi\equiv m\phi$ with a scalar potential $V(\Phi)\equiv\lambda m^4U(\phi)$, where ϕ, λ, and U are all dimensionless and m has dimensions of mass. (Here and throughout, we use units where $\hbar=k_B=c=1$ and $m_{\rm Pl}=1.2\times10^{19}$ GeV$=G_{\rm Newton}^{-1/2}$ is the Planck mass.) Stable domain walls occur when $U(\phi)$ has at least two degenerate minima. We consider two such potentials, sine-Gordon (SG) and ϕ^4:

$$U(\phi)=\begin{cases}1-\cos\theta, & \text{SG}\ ,\\ \frac{1}{2}(\phi^2-1)^2, & \phi^4\ .\end{cases}\tag{2.1}$$

Note that while the SG potential has an infinite series of minima ($\phi_{\rm min}=2\pi n$, where $n=$integer) and is bounded [$0\le U(\phi)\le2$ for all ϕ], the ϕ^4 theory has only two minima ($\phi_{\rm min}=\pm1$) and is unbounded [$U(\phi)\to\infty$ for $|\phi|\to\infty$].

Given the Lagrange density,

$$\mathcal{L}=\frac{m^2}{2}\partial_\mu\phi\partial^\mu\phi-\lambda m^4U(\phi)\ ,\tag{2.2}$$

we can easily derive the equation of motion for Φ:

$$\ddot{\phi}-\nabla^2\phi+\lambda m^2\frac{\partial U}{\partial\phi}=0\ .\tag{2.3}$$

Here and throughout an overdot will denote a derivative with respect to time. For a static, plane-symmetric domain wall oriented in the x-y plane, Eq. (2.3) simplifies to

$$\frac{d^2\phi}{dz^2}=\lambda m^2\frac{\partial U}{\partial\phi}\ .\tag{2.4}$$

Integrating, we find

$$\frac{1}{2}\left[\frac{d\phi}{dz}\right]=\lambda m^2U(\phi)\ .\tag{2.5}$$

A static, plane-symmetric wall is a solution of this equation with the boundary condition that ϕ approaches different minima for $z\to\pm\infty$. Evidently, the energy density inside the wall is $O(\lambda m^4)$, the thickness of the wall is $O(T)$, where $T\equiv1/\lambda^{1/2}m$, and the mass per unit area σ is $O(\lambda^{1/2}m^3)$. From Eq. (2.5) it follows that the stress tensor

$$T_{\mu\nu}=m^2\partial_\mu\phi\partial_\nu\phi-\eta_{\mu\nu}\mathcal{L}\tag{2.6}$$

takes the simple form

$$T_{\mu\nu}=2\lambda m^4U(\phi)\,\mathrm{diag}(-1,1,1,0)\ .\tag{2.7}$$

The closed-form solutions for ϕ in both SG and ϕ^4 theories are well known and we list them here for future reference:

$$\phi=\begin{cases}4\arctan(e^{m\lambda^{1/2}\gamma(z-Z_0-vt)}), & \text{SG}\ ,\\ \tanh[\lambda^{1/2}m(z-Z_0-vt)], & \phi^4\ .\end{cases}\tag{2.8}$$

Here v is the velocity of the wall in the z direction and $\gamma\equiv1/\sqrt{1-v^2}$ is the usual Lorentz factor. Using these results we find that $\sigma=8\lambda^{1/2}m^3$ for SG walls and $\sigma=4\lambda^{1/2}m^3/3$ for ϕ^4 walls.

Before discussing thick spherical and cylindrical walls let us consider these configurations in the thin-wall approximation. As noted above, a wall of negligible thickness is most easily described as a $(2+1)$-dimensional hypersurface. The motion of the wall is determined by the equations $x^\mu=x^\mu(\xi^a)$, where ξ^a ($a=0,1,2$) are the hypersurface coordinates and x^μ are the usual spacetime coordinates. The equations of motion for the wall are

$$\frac{\partial}{\partial\xi^a}\frac{\delta L}{\delta x^\mu{}_{,a}}-\frac{\delta L}{\delta x^\mu}=0\ ,\tag{2.9}$$

where $x^\mu{}_{,a}\equiv\partial x^\mu/\partial\xi^a$, $L\equiv-\sigma(-\det g^{(3)})^{1/2}$ is the Lagrangian of the wall, and $g^{(3)}_{ab}=g_{\mu\nu}x^\mu{}_{,a}x^\nu{}_{,b}$ is the metric on the hypersurface. For a spherically symmetric wall, we choose $x^\mu=(t,r,\theta,\phi)$ with

$$t=\xi^0,\quad r=R(\xi^0),\quad \theta=\xi^1,\quad \phi=\xi^2\ .\tag{2.10}$$

From this, and Eq. (2.9), it is straightforward to show that

$$\ddot{R}=-2\frac{1-\dot{R}^2}{R} . \tag{2.11}$$

Integrating this equation gives

$$1-\dot{R}^2=\left[\frac{R}{R_0}\right]^4 , \tag{2.12}$$

where $R_0=(M/4\pi\sigma)^{1/2}$ is the maximum size of the wall and M is the mass of the shell. [Equations (2.11) and (2.12) have also been derived[11] for thick walls, where R is replaced by an appropriately defined average radius.]

For cylindrical walls, we take $x^\mu=(t,\rho,\phi,z)$ with

$$t=\xi^0, \quad \rho=P(\xi^0), \quad \theta=\xi^1, \quad z=\xi^2 . \tag{2.13}$$

Again, making use of Eq. (2.9) we find

$$\ddot{P}=-\frac{1-\dot{P}^2}{P} \tag{2.14}$$

and

$$1-\dot{P}^2=\left[\frac{P}{P_0}\right]^2 . \tag{2.15}$$

Here $P_0=N/2\pi\sigma$ is the maximum radius of the cylinder and N is the mass per unit length of the shell.

For thick walls, we begin by writing Eq. (2.3) in spherical and cylindrical coordinates:

$$\ddot{\phi}-\frac{d^2\phi}{dr^2}-\frac{2}{r}\frac{d\phi}{dr}+\lambda m^2\frac{\partial U}{\partial\phi}=0 , \tag{2.16a}$$

$$\ddot{\phi}-\frac{d^2\phi}{d\rho^2}-\frac{1}{\rho}\frac{d\phi}{d\rho}+\lambda m^2\frac{\partial U}{\partial\phi}=0 . \tag{2.16b}$$

Numerical solutions of these equations will be discussed in Sec. III. Here we discuss the validity of the thin-wall approximation. The naive expectation is that the thin-wall approximation is valid so long as the radius of the sphere is much greater than the wall's thickness. This, however, is not the case. Consider a spherical wall that is initially at rest with a characteristic radius R_0 ($\gg T$). In the early stages of collapse, we expect, and indeed find in the numerical simulations, that the wall collapses with a speed determined by the relation $\gamma\propto R^{-2}$ [Eq. (2.12)]. Furthermore, the radial profile of the wall is approximately that of a planar wall that is Lorentz boosted with the appropriate γ factor [see Eq. (2.8)]. These properties hold so long as the third term on the left-hand side of Eq. (2.16a) is small as compared to the other terms in the problem. Comparing this term with, for example, the last term on the left-hand side, we see that

$$\frac{(2/r)d\phi/dr}{\lambda m^2\partial U/\partial\phi}\sim\frac{\gamma}{R\lambda^{1/2}m}\sim\left[\frac{R_0}{R}\right]^3\frac{T}{R_0} . \tag{2.17}$$

We, therefore, expect the thin-wall approximation to break down at a radius R_*, where

$$\frac{R_*}{R_0}\sim\left[\frac{T}{R_0}\right]^{1/3} . \tag{2.18}$$

Evidently R_* can be much larger than T. A similar analysis shows that, in the case of cylindrical symmetry, the thin-wall approximation breaks down when the radius of the cylinder is P_*, where

$$\frac{P_*}{P_0}\sim\left[\frac{T}{P_0}\right]^{1/2} . \tag{2.19}$$

As will be discussed below, Eqs. (2.18) and (2.19) are in good agreement with the numerical results.

III. NUMERICAL SIMULATIONS

The dynamics of thick domain walls are studied by solving the equation of motion for Φ choosing initial configurations appropriate to the problems we wish to consider. The equations are integrated numerically using a standard leapfrog finite-differencing scheme (see, for example, Ref. 12). Let ϕ_i^n denote the value of the field at the ith position and nth time step and $\dot{\phi}_i^{n+1/2}$ denote the first time derivative of the field again at the ith position but a half time step later. The difference equations are

$$\phi_i^{n+1}=\phi_i^n+\Delta t\,\dot{\phi}_i^{n+1/2} , \tag{3.1a}$$

$$\dot{\phi}_i^{n+1/2}=\dot{\phi}_i^{n-1/2}+\Delta t\left[\nabla^2\phi_i^n-\lambda m^2\frac{\partial V}{\partial\phi_i^n}\right] . \tag{3.1b}$$

For plane-symmetric configurations

$$(\nabla^2\phi)_i=\frac{\phi_{i+1}+\phi_{i-1}-2\phi_i}{(\Delta x)^2} . \tag{3.2a}$$

In the case of spherical symmetry

$$(\nabla^2\phi)_i=\frac{(\phi_{i+1}-\phi_i)(r_{i+1}+r_i)^2-(\phi_i-\phi_{i-1})(r_i+r_{i-1})^2}{(2r_i\Delta x)^2} , \tag{3.2b}$$

where $r_i=i\Delta x$. Finally, for problems with cylindrical symmetry

$$(\nabla^2\phi)_i=\frac{(\phi_{i+1}-\phi_i)(\rho_{i+1}+\rho_i)-(\phi_i-\phi_{i-1})(\rho_i+\rho_{i-1})}{2\rho_i(\Delta x)^2} . \tag{3.2c}$$

The differencing scheme is second-order accurate in both space and time.

We begin by discussing the interaction of plane-symmetric walls. This case corresponds to the interactions of (1+1)-dimensional kink solitons and has been studied elsewhere.[12,13] Here we briefly review the results. Our initial configuration is that of two widely separated walls (separation $\gg$ thickness) approaching each other with some velocity v. For the SG walls (Fig. 1), we find, as is well known, that the walls pass through one another without loss of coherence, continuing on with the same velocity as they started with. On the other hand, ϕ^4 solitons interact during a collision. The interaction is attractive so that the velocity after the collision is less than the initial velocity. If the relative velocity is small enough, then the walls will become bound and eventually annihi-

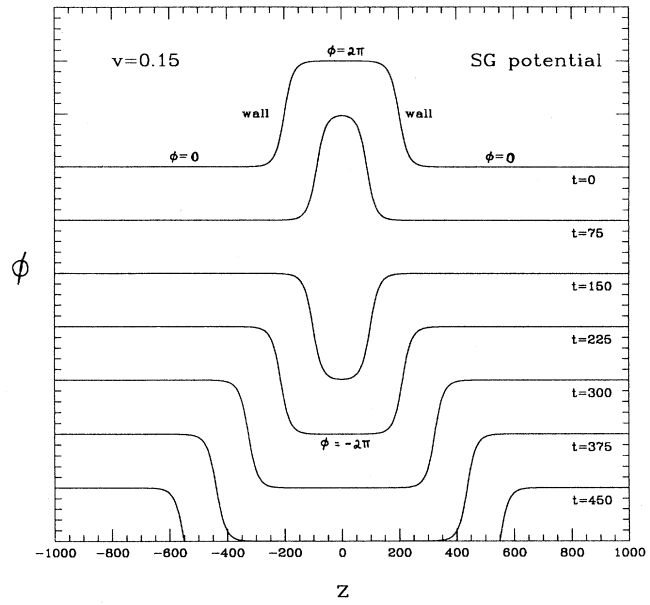

FIG. 1. Collision of two plane-symmetric SG walls. ϕ is shown as a function of z, the coordinate perpendicular to the plane of the wall, at different times during the collision. Time progresses as we move from the top of the figure to the bottom. Initially, the walls are moving towards one another with velocity $v=0.15$. $\phi\to 0$ for $|z|\to\infty$ while between the walls, $\phi=2\pi$. The walls pass through one another, and the region between the walls changes to $\phi=-2\pi$. The walls continue to move apart at $v=0.15$, their shape is unaffected by the collision, except for the reflection about $\phi=0$.

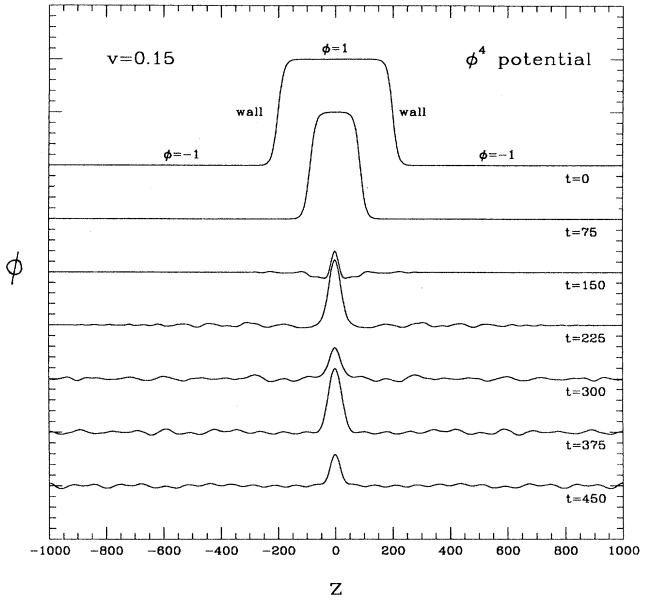

FIG. 2. Same as Fig. 1 but for ϕ^4 walls. Here, the walls interact during the collision. The kinetic energy in the walls is converted to scalar wave energy and the walls annihilate one another.

late one another (Fig. 2).

Now consider the collapse of spherically symmetric domain walls (Figs. 3 and 4). As initial conditions, we choose

$$\phi=\begin{cases}4\arctan(e^{m\lambda^{1/2}(r-R_0)}), & \text{SG}\ ,\\ \tanh[\lambda^{1/2}m(r-R_0)], & \phi^4\end{cases}\tag{3.3}$$

and $\dot{\phi}=0$, where $R_0\gg T$. (In Figs. 3 and 4 $T/R_0\simeq 0.04$.) These configurations correspond to spherical walls initially at rest with a characteristic radius R_0. For the purposes of the numerical simulations, we set $m=1$. In this way, all distances and times are measured in units of m^{-1}. We solve for ϕ in the region $r=[0,R_{\text{grid}}]$, where $R_{\text{grid}}\sim(2-4)R_0$ is the size of the grid used in the calculation. Initially the wall collapses with its inward radial velocity approximately given by Eq. (2.12). The radial profile of the wall has the shape of a one-dimensional kink that is being boosted to higher and higher velocities (i.e., the wall appears thinner due to length contraction). However, at $t\simeq 8$, the profile begins to deviate from that of a boosted kink. As the wall continues to collapse, it becomes less coherent so that by the time most of the wall energy has reached the origin ($t\simeq 12$), the field is undergoing large oscillations.

The evolution of the wall for $t\geq 12$ depends crucially on the details of the potential and the ratio T/R_0. Consider first the SG wall (Fig. 3). After collapse, a new wall forms and expands, reaching a maximum size at $t\simeq 20$. The wall then recollapses while a certain fraction of energy is radiated away in the form of outward traveling spherical waves. The loss of energy due to ϕ radiation is also evident in the fact that the new wall expands to a size that is somewhat less than the size of the original sphere. Figure 4 shows a ϕ^4 wall. Here all of the energy is radiated away after the first bounce. That is, the collapse of the ϕ^4 wall is perfectly inelastic.

Consider now, the collapse of a cylindrical SG wall (Fig. 5). Again we see a clear loss of coherence in the radial profile of the wall. However, unlike the spherical SG wall, all of the energy in the wall is converted to outgoing waves after the initial collapse.

One of the most striking observation of our simulations is that the radial profile of the wall deviates from the "kink" profile at a radius that is still fairly large as compared with the thickness of the wall. Though this was anticipated by Eqs. (2.18) and (2.19) there is still a worry that our results are reflecting some numerical instability. A number of facts, listed here, indicate that the code is working properly.

(1) Our solutions are independent of Δx and Δt.

(2) Energy is very nearly conserved during the course of a given run. Using $\sim 10^3$ zones across the grid and choosing $\Delta t=0.5\Delta x$ ($\frac{1}{2}$ the Courant condition) we find that energy is conserved to one part in 10^4.

(3) For a thin spherical (cylindrical) wall, $\gamma R^2=\text{const}$ ($\gamma P=\text{const}$) [cf. Eqs. (2.12) and (2.15)]. Thick walls collapse more slowly than thin ones indicating a breakdown of the thin-wall approximation. This point was anticipated in Sec. II [Eqs. (2.18) and (2.19)] and we can now

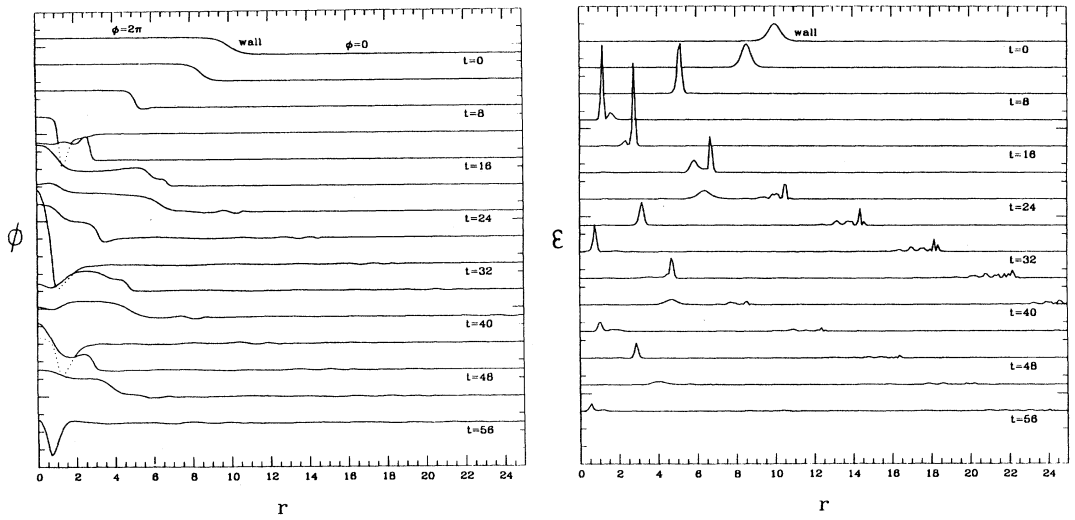

FIG. 3. Collapse of a spherically symmetric SG wall. r is the radial coordinate. The left-hand figure shows ϕ as a function of r at equally spaced intervals in time. On the right-hand side, we give the energy density ϵ for the corresponding time slices. (ϵ includes a factor of r^2 so that $\int dr\,\epsilon$ is the total energy.)

check these predictions numerically. Define R_* and γ_* by the relation $\gamma_* R_*^2 = 0.9 R_0^2$, i.e., R_* is the radius of the sphere at the point where γR^2 has dropped by 10%. Similarly, define P_* by the relation $\gamma_* P_* = 0.9 P_0$. In Fig. 6 we plot R_* and P_* as functions of T/R_0 and derive the empirical relations

$$\frac{R_*}{R_0} = 1.40 \left[\frac{T}{R_0} \right]^{0.31}, \quad \frac{P_*}{P_0} = 1.08 \left[\frac{T}{P_0} \right]^{0.46}$$

in good agreement with Eqs. (2.18) and (2.19).

IV. RESULTS

A. Energy loss due to particle radiation

One of the most striking phenomena discussed in Sec. III is the bounce of spherical walls. The bounce is most dramatically illustrated in Fig. 7. Here we plot the fraction of the total energy ($\equiv \mathcal{P}$) that is contained within a volume which encompasses the original wall. This is done for both SG and ϕ^4 walls where data are taken from

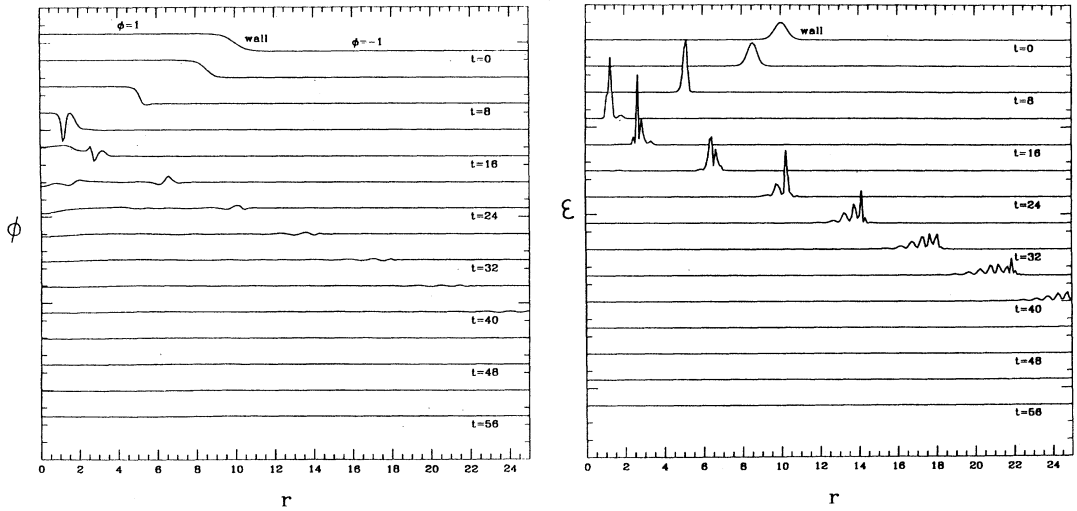

FIG. 4. Same as Fig. 3 but for a ϕ^4 wall.

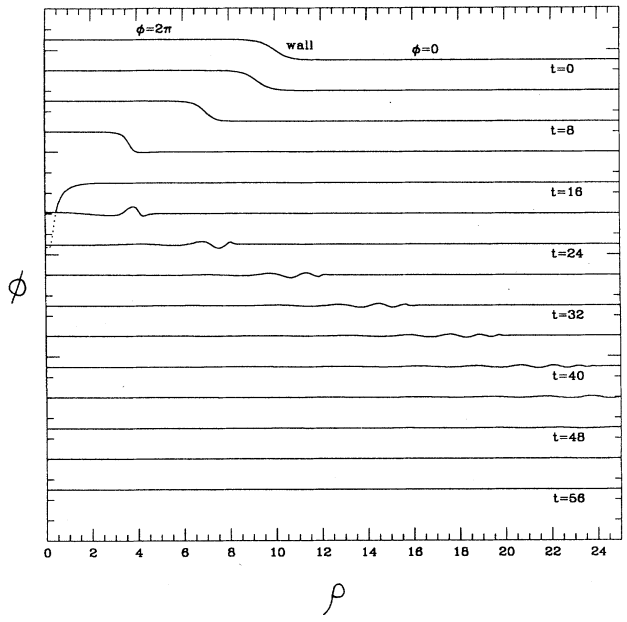

FIG. 5. Collapse of a SG wall that has cylindrical symmetry. ρ is the radial coordinate in the (t,ρ,ϕ,z) cylindrical coordinate system.

TABLE I. Values of C and x for different values of p in the power-law relation (4.1).

p	C	x
0.50	1.57	3.73
0.75	1.53	4.84
0.90	1.64	10.7
0.99	1.42	14.7

the same runs used in Figs. 3 and 4, respectively. The difference between the curves in Fig. 7 and the value 1 is a measure of the fraction of energy that has escaped in the form of outgoing spherical waves. We see that for the SG wall, roughly 40% of the energy is radiated away during each of the four or so bounces resolved in the plot. On the other hand, the ϕ^4 wall radiates all of its energy in the first bounce.

In Fig. 8 we plot $\mathcal{F}$ as a function of T/R_0. $\mathcal{F}$ is the fraction of the total energy in the wall that remains after the first bounce. We see that $\mathcal{F}$ reaches a maximum value of 0.7 (i.e., the collision is most elastic) at $T/R_0 \simeq 0.08$. The gross features of Fig. 8 have a fairly simple explanation. For $T/R_0 > 0.08$, the initial configuration begins to look like a dissipative blob of ϕ field rather than a spheri-

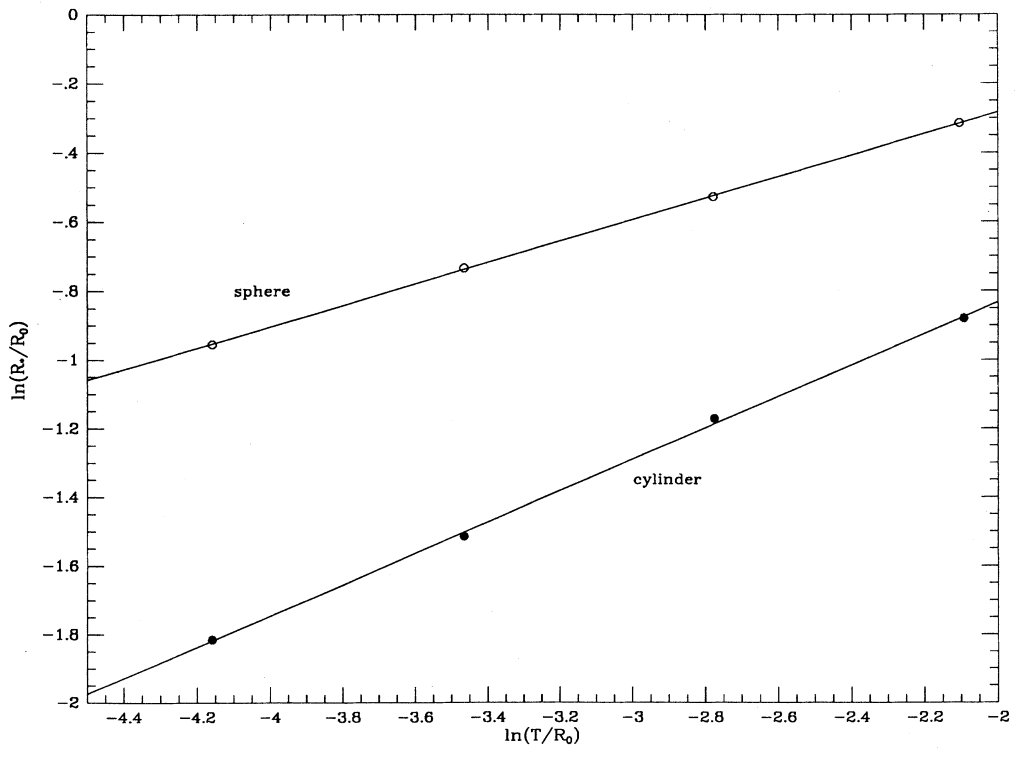

FIG. 6. Plot of $\ln(R_*/R_0)$ [$\ln(P_*/P_0)$] as a function of $\ln(T/R_0)$ for spherical [cylindrical] walls. R_* is the radius at which the thin-wall approximation first breaks down. (The exact definition of R_* is given in the text.) The straight line fit to the data [Eqs. (3.4a) and (3.4b)] is also shown.

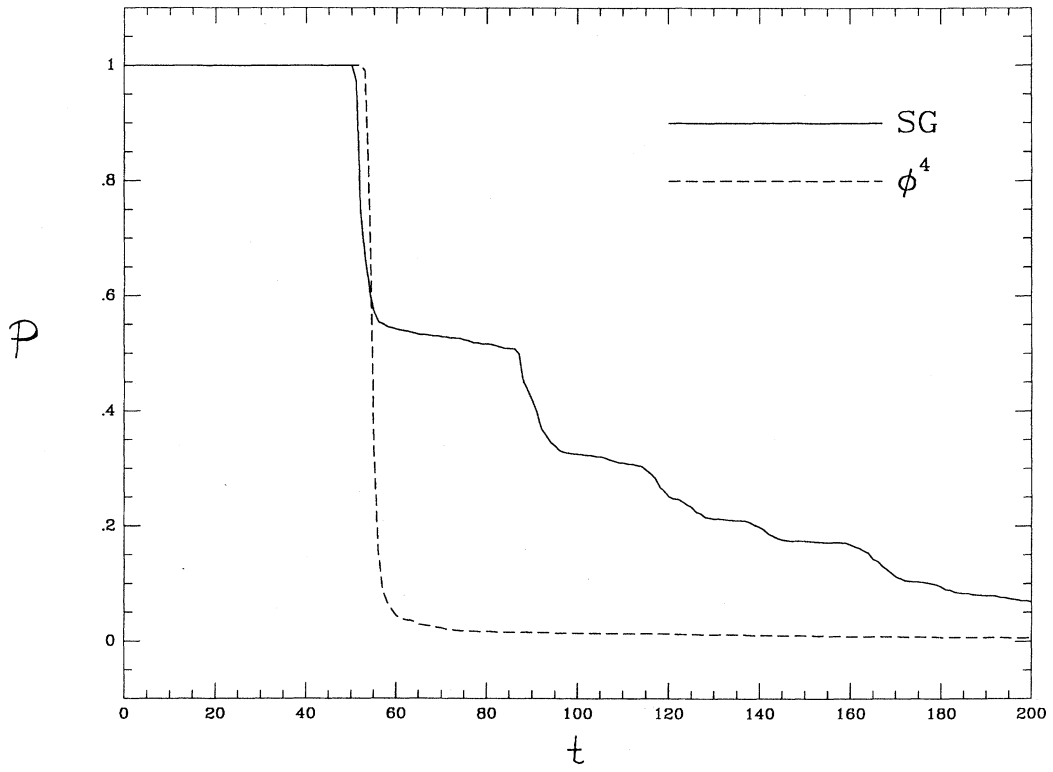

FIG. 7. Plot of $\mathcal{P}$ as a function of time. $\mathcal{P}$ is the fraction of energy contained in a region that encompasses the original wall. $1-\mathcal{P}$, therefore, measures the amount of energy that has escaped in the form of outward traveling scalar waves. Results are given for the SG and ϕ^4 runs used in Figs. 3 and 4.

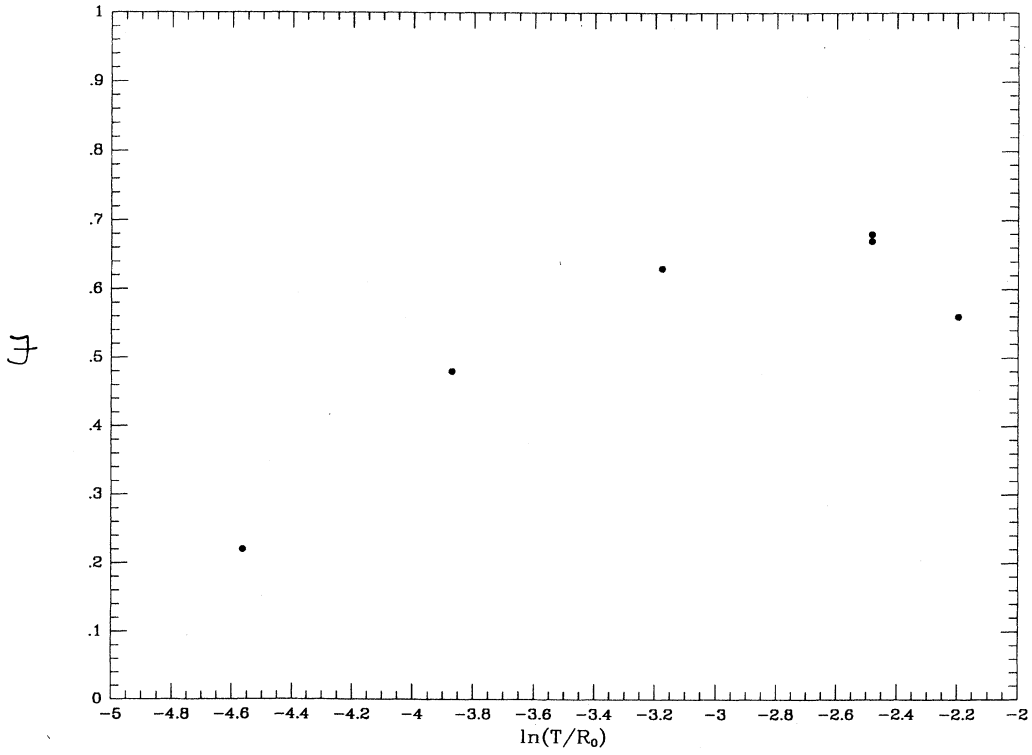

FIG. 8. $\mathcal{F}$ as a function of $\ln(T/R_0)$. $\mathcal{F}$ is the fraction of the total energy that remains as wall energy after the initial bounce.

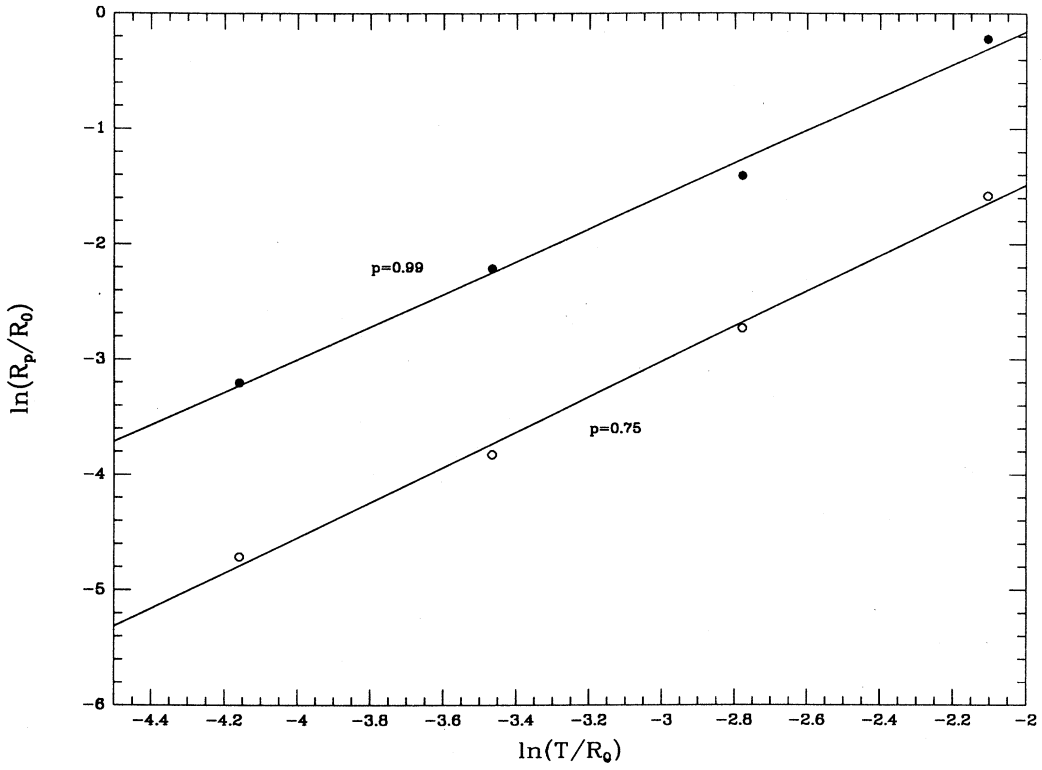

FIG. 9. $\ln(R_p/R_0)$ as a function of $\ln(T/R_0)$ for $p=0.75$ and $p=0.99$. R_p is the minimum radius in which a fraction p of the total energy can be compressed.

cal domain wall. Conversely, for T/R_0 much less than this, the radius at which the wall profile becomes incoherent as compared to the thickness R_*/T *increases* [see Eqs. (2.18) and (2.19)] indicating that the wall is undergoing larger oscillations by the time it reaches its final stages of collapse.

B. Black-hole formation

As in any problem involving spherical collapse, one should consider the possibility of black-hole formation. Since we have neglected gravity, an exact treatment of the gravitational collapse to a black hole is not possible. We can, however, make some (hopefully) sensible predictions about black-hole formation.

Define R_p to be the minimum radius that contains, during the course of the collapse, a fraction p of the total energy. We determine R_p/R_0 as a function of T/R_0 and display the results (for $p=0.75$ and $p=0.99$) in Fig. 9. The results are reasonably well approximated by the power-law relation

$$\frac{R_p}{R_0}=C\left[\frac{T}{R_0}\right]^x, \tag{4.1}$$

where C and x are given for different values of p in Table I.

Black holes form when a given amount of energy falls within its Schwarzschild radius, R_s. For a spherical wall $R_s=4\pi\sigma R_0^2/m_{\rm Pl}^2$. To form a black hole, we then require

$$\frac{R_p}{R_0}<\frac{4\pi p\sigma R_0}{m_{\rm Pl}^2} \tag{4.2a}$$

or

$$\frac{T}{R_0}<\left[\frac{4\pi p}{C}\left[\frac{m}{m_{\rm Pl}}\right]^2\right]^{1/(x+1)}. \tag{4.2b}$$

It is interesting to note that the condition for black-hole formation, Eq. (4.2b), depends on the ratio T/R_0 and m and not on λ. Even for the very light domain walls envisioned by HSF, m is a high-energy ($\sim 10^{16}$ GeV) scale. [The walls are light because $\lambda^{1/2}$, being the ratio of a low-energy scale ($\sim 1-10^{-2}$ eV) to m, is extremely small.] For $m=10^{16}$ GeV black holes are likely to form for $T/R_0\sim 10^{-2}$.

V. CONCLUSIONS

Phase transitions that involve spontaneous breaking of a discrete symmetry give rise to topological domain walls. Walls that are absolutely stable *and* heavy ($\sigma \geq 10$ MeV) induce unacceptably large distortions in the microwave background and theories that predict such objects must either be altered in some way (for example, by requiring inflation to occur after wall formation) or discarded. However, domain walls that are unstable *or* light are cosmologically safe and may even be cosmologically interesting. In order to determine just how safe and in-

teresting domain walls are one must understand the dynamical evolution of a domain-wall network. Here we study the details of spherical and cylindrical collapse as well as the collision of two plane-symmetric walls. Our simulations are extremely accurate (i.e., using a finer grid does not change the results) and reveal a number of interesting properties. For example, spherical SG walls can bounce after collapse, retaining a fair fraction of their energy in wall energy, losing the balance of the energy to ϕ radiation. This indicates that the lifetime of the walls is (a few)$\times$(light travel time across the wall). Subhorizon-sized walls can, therefore, live for a time $\leq$Hubble time making them acceptable (but just barely) as seeds for structure formation. (There is, however, the possibility that the lifetime of the wall can be enhanced if the wall has anisotropies or angular momentum, though the results of Press, Ryden, and Spergel[8] indicate that such walls are not very common.)

One very interesting, albeit preliminary, result is that black holes may form during spherical collapse. This could occur for domain walls that are heavy but unstable (as in the case where the discrete symmetry is only approximate). In such a scenario, a population of black holes could form before the walls have disappeared. This possibility will be the subject of a future investigation.

ACKNOWLEDGMENTS

It is a pleasure to thank William Press for many useful suggestions and comments. I would also like to thank the members of the Theory Group at the Center for Astrophysics and the Particle Theory and Astrophysics Groups at Fermilab for stimulating discussions. This work was supported, in part, by the National Science Foundation (Grant No. PHY-8604396) at Harvard.

[1]C. T. Hill, D. N. Schramm, and J. Fry, Comments Nucl. Part. Sci. (to be published).
[2]A. Stebbins and M. S. Turner, Astrophys. J. Lett. **339**, L13 (1989).
[3]A. Dressler *et al.*, Astrophys. J. Lett. **313**, L37 (1987); D. Burstein *et al.*, Astrophys. J. Suppl. **64**, 601 (1987).
[4]A. Vilenkin, Phys. Rep. **121**, 263 (1985).
[5]J. Ipser and P. Sikivie, Phys. Rev. D **30**, 712 (1984).
[6]See, e.g., V. A. Berezin, V. A. Kuzmin, and I. I. Tkachev, Phys. Rev. D **36**, 2919 (1987).
[7]L. M. Widrow, Phys. Rev. D **39**, 3576 (1989).
[8]W. H. Press, B. Ryden, and D. N. Spergel, Astrophys. J. (to be published).
[9]T. Vachaspati and A. Vilenkin, Phys. Rev. D **30**, 2036 (1984).
[10]H. Hodges, Phys. Rev. D **39**, 3557 (1989).
[11]V. Silveira, Phys. Rev. D **38**, 3823 (1988).
[12]W. H. Press, B. P. Flannery, S. A. Teukolsky, and W. T. Vetterling, *Numerical Recipes: The Art of Scientific Computing* (Cambridge University Press, New York, 1986).
[13]M. J. Ablowitz, M. D. Kruskal, and J. F. Ladik, SIAM J. Appl. Math. **36**, 428 (1979).